# Ab Initio Study of Chiral Discrimination in the Glycidol Dimer

Reza Hemmati<sup>1</sup> and Konrad Patkowski<sup>1,\*</sup>

<sup>1</sup>Department of Chemistry and Biochemistry, Auburn University, Auburn, AL 36849 (Dated: October 15, 2020)

#### Abstract

Chiral discrimination, the ability of a chiral molecule to exhibit different weak intermolecular interactions than its mirror image, is investigated for dimers of oxiranemethanol (glycidol). In this regard, high level ab initio calculations were performed to study the chiral recognition effects in the homochiral and heterochiral dimers of glycidol. 14 dimer structures, seven homochiral and seven heterochiral, were studied: they all feature two intermolecular O-H···O hydrogen bonds. These structures have been determined with the second-order Møller-Plesset perturbation theory (MP2) using the aug-cc-pVTZ basis set, and verified to pertain to actual local minima. The benchmark interaction energy values were computed using MP2 extrapolated from the aug-cc-pVQZ and augcc-pV5Z bases with a higher-level correction from a coupled-cluster calculation in the aug-cc-pVTZ basis. The global-minimum structure is a homochiral one, with the two hydrogen bonds forming a part of a ring with 8 heavy atoms. A similar heterochiral structure has a binding energy smaller by about 0.6 kcal/mol. The largest diastereomeric energy difference is about 1.0 kcal/mol. Further insight into the origins of chiral discrimination was provided by symmetry-adapted perturbation theory (SAPT), and a functional-group SAPT (F-SAPT) difference analysis to investigate the direct and indirect effects of two -H/-CH<sub>2</sub>OH substitutions leading from an achiral ethylene oxide dimer to the chiral glycidol dimer. Last but not least, harmonic frequency shifts relative to a noninteracting glycidol molecule were calculated and analyzed for all conformations in order to get insight into the origins of chiral discrimination. It is found that the largest frequency shifts are related to the effect of hydrogen bonding on the O-H stretch mode, the stability of the ring involving both hydrogen bonds, and the transition between two nonequivalent minima of the glycidol molecule.

#### I. INTRODUCTION

Investigating and understanding weak intermolecular interactions involving chiral molecules is of great importance in biology and drug design. The two forms of a chiral molecule have the same chemical and physical properties, but they interact differently with other chiral molecules which in turn leads to distinctive chiral recognition effects. A key feature to examine is chiral discrimination energy, which is defined as the energy difference between diastereomers. In the specific case of two identical chiral molecules, the chiral discrimination energy differentiates between a homochiral (RR/SS) and its counterpart heterochiral complex (RS/SR). The homochiral nature of the living organisms that almost exclusively use L-amino acids, D-sugars, and L-phospholipids, makes molecular chiral discrimination a highly significant research topic in chemistry and biology. Moreover, the energetic and conformational differences between diastereomeric complexes may lead to privileged binding of one enantiomer over the other; this is the cornerstone of enantioselectivity in organic synthesis. The preferential production of one enantiomer is a highly sought after goal of enantioselective synthesis, and has ultimately led to the observed homochirality of life through countless cycles of enantioselective processes, even though the source of the initial small enantiomeric excess might have been quite different<sup>1</sup>. A detailed description of the underlying intermolecular interactions of chiral diastereomers, leading to the chiral discrimination effects, is not yet fully established. This paper aims to provide such a first-principles description for a model diastereomeric complex, the glycidol dimer.

In the last few years, the chiral discrimination effects have been investigated<sup>2–9</sup>, theoretically and experimentally, for several representative gas-phase intermolecular complexes. The systems studied include glycidol dimer<sup>2</sup>, butan-2-ol dimer<sup>10</sup>, propylene oxide dimer<sup>4,8</sup>, and the propylene oxide-glycidol<sup>6</sup> complex. Techniques such as Fourier Transform Microwave (FTMW) spectroscopy have been applied to investigate the conformational and dynamical characteristics of several of these chiral complexes<sup>4,7</sup>. Moreover, some of the important vibrational modes of these complexes were analyzed by infrared spectroscopy<sup>2</sup>.

From a theoretical perspective, the chiral discrimination phenomenon is quite hard to study. First, the supermolecular interaction energies for individual complexes are computed as differences between the energy of the complex and the energies of the noninteracting molecules (monomers):

$$E^{\rm int} = E_{AB} - E_A - E_B. \tag{1}$$

Then, the chiral discrimination energy (chirodiastaltic energy), measuring the relative stability of the homo- and heterochiral complexes, is a difference of differences<sup>11</sup>:

$$\Delta E_{\rm chir}^{\rm int} = E_{\rm RR}^{\rm int} - E_{\rm RS}^{\rm int} \tag{2}$$

Even further, it might be advantageous to discuss the effect of various substituents on chiral discrimination, and one can examine the variation of  $\Delta E_{\rm chir}^{\rm int}$  between the substituted and unsubstituted monomers, leading to differences of differences of differences. It is well known that computing interaction energies accurately requires not just a size-consistent method to allow for error cancellation between  $E_{AB}$  and  $E_A + E_B$ , but an accurate, high-level account of electron correlation and, at the same time, a large enough basis set to overcome the slow convergence of electron correlation effects such as dispersion. The coupled-cluster approach with single, double, and perturbative triple excitations, CCSD(T), has been the method of choice to generate benchmark high-accuracy interaction energies, and the basis set requirements for calculating values sufficiently converged to the CCSD(T) complete basis set limit (CBS) have been well established 12,13. It is quite likely that a carefully selected more approximate approach, such as a variant of density functional theory (DFT), might exhibit consistent error cancellation and provide accurate  $\Delta E_{\rm chir}^{\rm int}$  values for all systems relevant to a particular study, but such behavior should never be taken for granted and a comparison to CCSD(T)-level benchmark values is required for validation.

An additional drawback of the supermolecular method, Eqs. (1)–(2), is that the resulting numbers,  $E^{\rm int}$  and  $\Delta E^{\rm int}_{\rm chir}$ , provide little insight into the origins of the chiral discrimination. Therefore, it is advantageous to supplement supermolecular calculations with ones that provide some form of interaction energy decomposition. Symmetry-adapted perturbation theory (SAPT)<sup>14–16</sup> can provide both accurate total interaction energies and a meaningful energy decomposition. Moreover, a finer-grained partitioning of SAPT corrections is afforded by the functional-group SAPT (F-SAPT) modification<sup>17</sup>, where each SAPT term (electrostatics, induction, dispersion, and exchange) is further split into contributions originating from a specific pair of functional groups on the two molecules. F-SAPT has been applied to provide unique insight into several problems of practical interest, from the origins of substituent effects in  $\pi - \pi$  stacking<sup>18</sup> to the stabilization of a specific transition state stereoisomer in some organocatalyzed reactions<sup>19,20</sup>.

Very recently, the SAPT and F-SAPT decompositions have been applied to elucidate the origins of chiral discrimination. In our previous study<sup>8</sup>, the interactions between two propylene oxide (PO) molecules led to 12 dimer conformations which represented six homochiral and six heterochiral local minima. The coupled-cluster, DFT, SAPT, and F-SAPT approaches were utilized to compute the PO-PO intermolecular interaction energies. In contrast with

the current study, propylene oxide is a very rigid molecule: the monomer deformation energy was minuscule and could be ignored in all calculations. Some "DFT plus dispersion" variants, especially B3LYP-D3 and B3LYP-D3M<sup>21</sup>, performed very well on this system. The results of other methods such as SAPT showed a systematic overbinding of all dimer structures, but the SAPT2+3 approach<sup>22</sup> overbinds much less than the more approximate SAPT0 level, mainly because of the inclusion of intramolecular correlation effects in the first-order exchange-repulsion term. The analysis of SAPT results showed that the main origin of binding in the PO-PO dimers is dispersion followed by electrostatics. The F-SAPT analyses showed that the direct effects of the -H/-CH<sub>3</sub> substitution dominate over the indirect effects resulting from the electron density change in the rest of the molecule. Last but not least, vibrational frequency calculations were performed on the 12 PO-PO structures to investigate the frequency shifts, splittings, and chiral differences. The modes most affected by the noncovalent interactions are the lowest-frequency mode coming from the methyl group rotation and some specific C-H and C-C stretching modes.

Another study<sup>9</sup> from last year, similar to ours in methods but different in molecular systems, gives deep insights into the applicability of F-SAPT and other methods to chiral recognition effects. Korona and coworkers performed a comprehensive study on three chiral drug molecules, ibuprofen, norepinephrine, and baclofen, with two chiral phases of phenethylamine and proline. They concluded that the interaction energy differences between the RR and RS complexes are significant for structures containing phenethylamine but not necessarily for those with proline. Another study of the same group<sup>23</sup> examined the dimerization process of methyl chlorophyllide a, and the F-SAPT analysis showed the crucial role of the magnesium ions in the stabilization of the dimer.

As the chiral monomer for the present study, glycidol was chosen for two main reasons. First, it has a polar hydroxyl group that can rotate around the C-O bond, which gives an opportunity to explore the influence of monomer deformation on the chiral discrimination effects. Second, it is a relatively small molecule that can be used as a prototype for bigger molecular systems, and the glycidol dimer can be studied accurately using high-level electronic structure methods. In this work, we aim at a quantitative analysis of the origins of chiral discrimination in the glycidol dimers at the molecular level. To this end, we first determine accurate CCSD(T)-level benchmark interaction energies that can in turn be used to assess the accuracy of more approximate methods such as different flavors of DFT with dispersion. Similar to our earlier PO-PO study<sup>8</sup>, we then reveal the details of the chiral discrimination process using SAPT, F-SAPT, and a differential F-SAPT analysis of the effects of replacing hydrogen atoms by the -CH<sub>2</sub>OH groups, going from an achiral ethylene oxide dimer to the chiral glycidol dimer.

Glycidol possesses two functional groups: a rigid oxirane ring and a methanol unit. Therefore, it is able to form both intra- and intermolecular hydrogen bonds. The intramolecular interaction of the hydroxyl group with the oxirane ring has been studied previously by  $\bar{O}$ ki and Murayama<sup>24,25</sup>. The two lowest energy conformers denoted by M1 and M2 (Fig. 1) were identified in the infrared spectroscopic study<sup>26</sup> and between these two, M1 is the global minimum structure. For the glycidol dimers, some conformers have been studied spectroscopically by Caminati and co-workers<sup>7</sup>, who also identified the remaining local minima (for a total of 7 homochiral and 7 heterochiral ones) using MP2/6-311++G\*\* calculations.

This article is organized as follows: in Section II, we describe the theoretical background; in Section III, the results and their discussion are given; and the summary follows in Section IV.

### II. METHODS AND COMPUTATIONAL DETAILS

We considered 14 dimer structures, initially proposed in Ref. 7, with two glycidol subunits held together through weak intermolecular interactions. Among these structures, there are seven homochiral dimers labeled "HOM" consisting of two R or two S subunits, and seven heterochiral dimers which are labeled "HET" arising from a complex between an R enantiomer and an S one. These complexes can be additionally divided into two groups according to Borho and Suhm<sup>2</sup>, as shown in Fig. 1. One group forms hydrogen bonds which involve a ring of eight heavy atoms and is labeled by "8" in addition to either HOM or HET. In the second group, the hydrogen bonds form a ring involving only five heavy atoms, and it is labeled "5". In each 8-membered ring structure, each glycidol monomer serves as a donor for one O-H···O hydrogen bond and as an acceptor for the second hydrogen bond with the involvement of both its oxygen atoms. However, in 5-membered ring systems, a single OH group in one of the glycidol monomers acts as a hydrogen bond donor and an acceptor at the same time, as illustrated in Fig. 1. The last two-digit coding in the name of a structure denotes the type of monomer conformation which is shown in the top left of Fig. 1. There is a caveat for some 5-membered ring structures: in order to distinguish the minima involving a five-membered ring and one monomer in each conformation, we call them HOM512, HET512, HOM521, and HET521. The ordering of digits indicates that in HOM512, as an example, one functional group of M1 and two functional groups of M2 are involved in the hydrogen bonding, while in HOM521 two functional groups of M1 and one functional group of M2 form hydrogen bonds. The same applies to HET512 and HET521.

All 14 geometries of the glycidol dimer were reoptimized starting from the initial structures taken from Ref. 7,

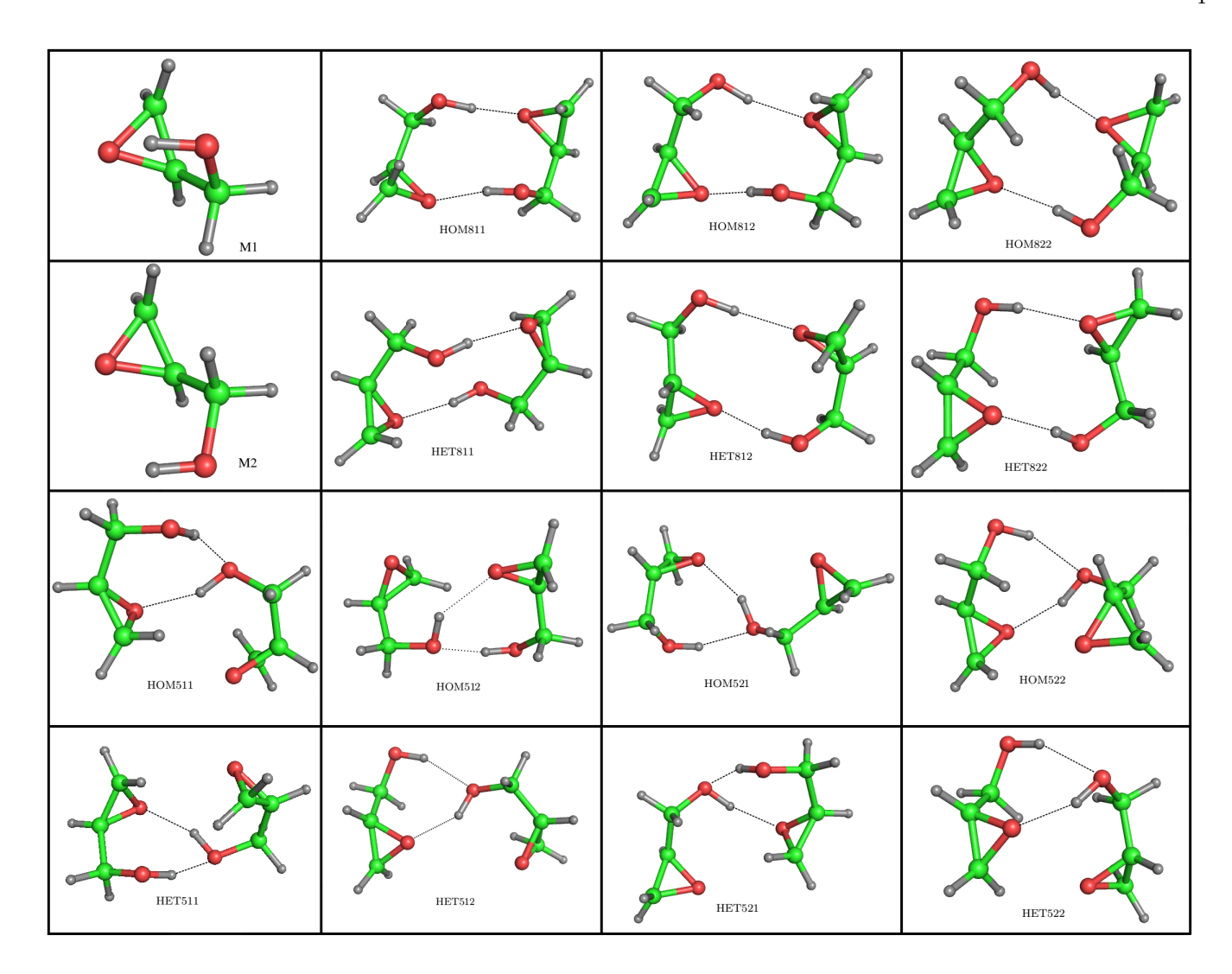


FIG. 1: Optimized geometries of 7 homochiral (HOM) and 7 heterochiral (HET) conformers of the glycidol dimer obtained at the DF-MP2/AVTZ level. The two monomer conformations M1 (global minimum) and M2 are also shown. The structures are grouped in pairs corresponding to the same patterns of hydrogen bonding and monomer conformations.

where they were obtained at the MP2/6-311++G\*\* level. We reoptimized them using the DF-MP2/AVTZ level, where AVTZ=aug-cc-pVTZ denotes the augmented correlation consistent triple-zeta Dunning basis<sup>27,28</sup>. While the structures used in all single-point energy calculations were obtained by minimizing the counterpoise-corrected interaction energy including the monomer deformation corrections, for the frequency calculations, one must use a structure that minimizes the total dimer energy rather than the interaction energy. Such a change in the optimization target resulted in insignificant changes to the geometry, and the frequency calculations confirmed that each of the 14 structures is a local minimum.

The counterpoise-corrected supermolecular approach, Eq. (1), has been applied to the electronic structure methods used in this work, with all three quantities  $E_{AB}$ ,  $E_{A}$ , and  $E_{B}$  computed in the full dimer basis set. Our benchmark interaction energies are the composite DF-MP2/(AVQZ,AV5Z)+ $\Delta$ CCSD(T)/AVTZ values, where the  $\Delta$ CCSD(T) term represents the difference between the CCSD(T) and MP2 interaction energies computed with a desired basis set:

$$\Delta E_{\rm int}^{\rm CCSD(T)} = E_{\rm int}^{\rm CCSD(T)} - E_{\rm int}^{\rm MP2}. \tag{3}$$

Also, to quantify the accuracy of various approximate methods relative to benchmark, the mean unsigned errors

(MUE) relative to reference values have been computed using the following formula<sup>29</sup>.

$$MUE = \frac{\sum_{i=1}^{n} |E_{\text{method}}^{i} - E_{\text{benchmark}}^{i}|}{n},$$
(4)

where n is the size of the data set. The MUE statistics were obtained for a number of approximate methods, mostly based on density functional theory DFT. The DFT calculations utilized the functionals B3LYP, BLYP, PBE, and PBE0 with the atom-pairwise dispersion corrections in the -D3 $^{30}$ , -D3(BJ) $^{31}$ , -D3M, and -D3M(BJ) $^{21}$  variants. All calculations in this work have been performed using the MOLPRO $^{32}$  and PSI4 $^{33}$  programs.

The SAPT approach<sup>14–16</sup> offers a systematic way to calculate intermolecular interaction energies decomposed into physically meaningful components, and we used SAPT to analyze the glycidol-glycidol interactions. In SAPT, the interaction energy is calculated directly as a sum of terms in the perturbative series. In our case, this sum extends through the second-order in the intermolecular interaction operator:

$$E_{\text{int}}^{\text{SAPT}} = \left(E_{\text{elst}}^{(1)}\right)_{\text{elst}} + \left(E_{\text{exch}}^{(1)}\right)_{\text{exch}} + \left(E_{\text{ind,resp}}^{(2)} + E_{\text{exch-ind,resp}}^{(2)} + \delta E_{\text{HF}}\right)_{\text{ind}} + \left(E_{\text{disp}}^{(2)} + E_{\text{exch-disp}}^{(2)}\right)_{\text{disp}},$$

$$(5)$$

where the order of each component is represented by its superscript and the groupings of terms into the four commonly used SAPT contributions are indicated by parentheses. The first two of these contributions are the first-order electrostatic and exchange energy components, respectively, and the next two are the second-order induction and dispersion terms together with their exchange counterparts. The  $\delta E_{\rm HF}$  term in Eq. (5) represents the remaining higher-order induction components approximated using a supermolecular Hartree-Fock (HF) calculation as

$$\delta E_{\rm HF} = E_{\rm int}^{\rm HF} - E_{\rm elst}^{(10)} - E_{\rm exch}^{(10)} - E_{\rm ind,resp}^{(20)} - E_{\rm exch-ind,resp}^{(20)},\tag{6}$$

where the second "0" in the superscript indicates that the intramolecular correlation effects have been neglected, as done at the SAPT0 level of theory  $^{16,22}$ . In this work, we will employ two levels of SAPT: the simplest SAPT0 variant, neglecting intramolecular correlation, and the much more sophisticated SAPT2+3 one including a large variety of intramolecular correlation effects through second order as well as the leading intermolecular interaction effects through third order  $^{22}$ . In addition to conventional SAPT, we add another layer of useful information and insight by employing the functional-group-pairwise partitioning denoted as F-SAPT $^{17,34}$ . F-SAPT decomposes each SAPT0 interaction energy component into contributions arising from the interaction of a given functional group on monomer A with a particular functional group on monomer B. The F-SAPT analysis is based on the key assumption that the functional groups are chemically separable units connected by only single  $\sigma$  bonds  $^{17}$ . Accordingly, we separate each glycidol monomer into two units, the -CH<sub>2</sub>OH functional group and the -C<sub>2</sub>H<sub>3</sub>O backbone.

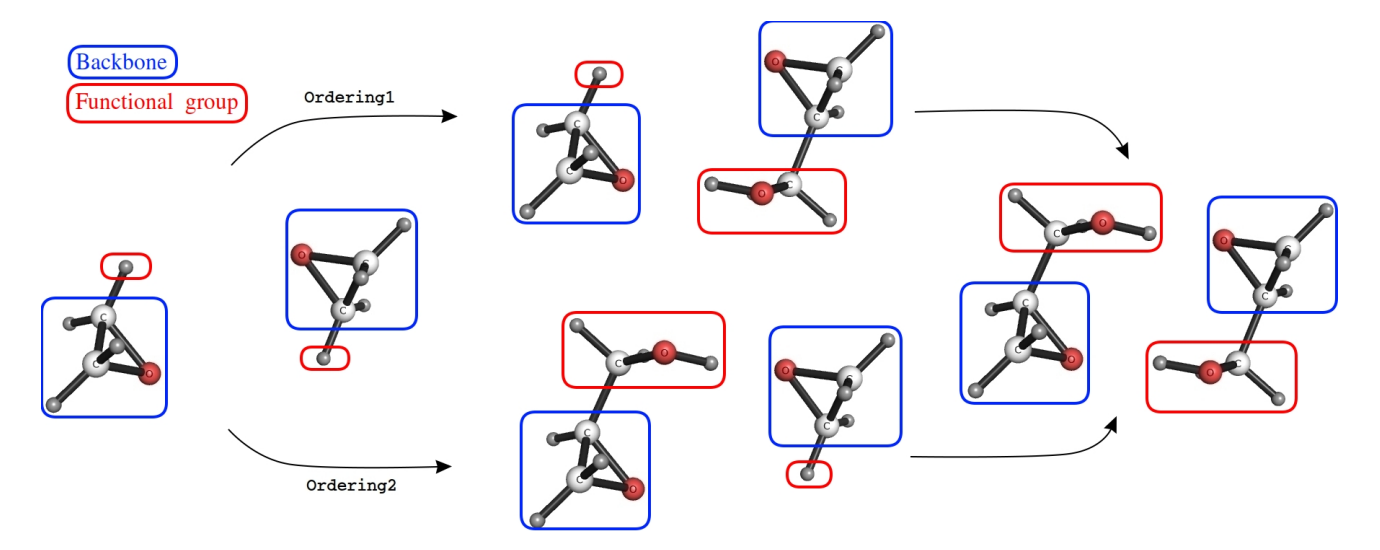


FIG. 2: Two different pathways leading to a chiral glycidol dimer structure from an achiral ethylene oxide dimer structure, and the fragmentation pattern in the F-SAPT calculations.

The fragmentation scheme applied for the glycidol dimer is shown in Fig. 2. This figure also illustrates another layer of abstraction in the form of the F-SAPT difference analysis <sup>19,20,34</sup>. In the current study, we are interested in the substituent effects on the F-SAPT interaction energy components across a class of similar systems. For this reason, similar to our earlier study<sup>8</sup>, we started with the (achiral) ethylene oxide (EO) dimer and substituted the -CH<sub>2</sub>OH functional groups in two consecutive steps, replacing a hydrogen atom in each ethylene oxide monomer in order to arrive at a glycidol dimer structure. In this manner, a particular SAPT component of the glycidol–glycidol (GL-GL) interaction in a given homo- or heterochiral structure is partitioned as

$$E_{\text{GL-GL}}^{\text{SAPT}} = E_{\text{EO-EO}}^{\text{SAPT}} + \Delta_{\text{SAPT}}(\text{EO-GL}) + \Delta_{\text{SAPT}}^{1}(\text{GL-GL}), \tag{7}$$

and

$$E_{\rm GL-GL}^{\rm SAPT} = E_{\rm EO-EO}^{\rm SAPT} + \Delta_{\rm SAPT}(\rm GL-EO) + \Delta_{\rm SAPT}^{2}(\rm GL-GL), \tag{8}$$

depending on which monomer accepts the substituent hydroxymethyl group first. In Eqs. (7) and (8),  $\Delta_{\text{SAPT}}(\text{EO}-\text{GL}) = E_{\text{EO}-\text{GL}}^{\text{SAPT}} - E_{\text{EO}-\text{GL}}^{\text{SAPT}} - E_{\text{EO}-\text{EO}}^{\text{SAPT}}$ ,  $\Delta_{\text{SAPT}}(\text{GL}-\text{GL}) = E_{\text{GL}-\text{GL}}^{\text{SAPT}} - E_{\text{EO}-\text{GL}}^{\text{SAPT}}$ ,  $\Delta_{\text{SAPT}}(\text{GL}-\text{EO}) = E_{\text{GL}-\text{EO}}^{\text{SAPT}} - E_{\text{EO}-\text{EO}}^{\text{SAPT}}$ , and  $\Delta_{\text{SAPT}}^2(\text{GL}-\text{GL}) = E_{\text{GL}-\text{GL}}^{\text{SAPT}} - E_{\text{GL}-\text{EO}}^{\text{SAPT}}$  for any SAPT term. The ordering of the two glycidol monomers is arbitrary, but it is kept consistent in a pair of homo- and heterochiral structures.

The last quantities that we investigated were the normal modes of the 14 dimer structures, where we examined the frequency shifts to get more insight into the weak intermolecular interactions leading to chiral discrimination. The vibrational modes of all 14 glycidol dimer configurations were computed at the DF-MP2/AVTZ level of theory, and the frequency shifts were calculated with respect to the harmonic vibrational frequencies of an isolated glycidol monomer at its global minimum (M1 in Fig. 1). Every dimer structure has 60 normal modes, but six of them are low-frequency intermolecular motions and will not be considered further. The remaining 54 normal modes come in pairs (originating from the same monomer mode) and lead to two distinct frequency shifts pertaining to some combination of these modes in the two interacting monomers.

Table I: Benchmark DF-MP2/(AVQZ,AV5Z)+ $\Delta$ CCSD(T)/AVTZ interaction energies (in kcal/mol) for the glycidol dimer.

Structure	$\mathrm{DF\text{-}MP2/CBS}$	$\Delta {\rm CCSD}(T)$	Benchmark	$\Delta E_{ m chir}^{ m int}$ a				
HOM811	-14.499	0.144	-14.355	1.620				
HET811	-16.059	0.084	-15.975					
HOM812	-12.702	0.135	-12.567	-1.469				
HET812	-11.251	0.153	-11.098					
HOM822	-11.987	0.185	-11.802	-0.181				
HET822	-11.813	0.192	-11.621					
HOM511	-10.235	0.187	-10.048	1.474				
HET511	-11.663	0.142	-11.522					
HOM512	-10.154	0.174	-9.980	-0.093				
HET512	-9.998	0.111	-9.887					
HOM521	-10.374	0.115	-10.259	0.737				
HET521	-11.174	0.178	-10.996					
HOM522	-12.404	0.155	-12.249	-0.410				
HET522	-11.972	0.132	-11.839					
<sup>a</sup> Defined as $\Delta E_{\rm chir}^{\rm int} = E_{\rm homodimer}^{\rm int} - E_{\rm heterodimer}^{\rm int}$								

### III. RESULTS AND DISCUSSION

### A. Benchmark interaction and binding energies

In this section, we describe the results of various wavefunction and DFT methods and will see which ones perform well for our diastereomeric complexes. Table I presents the benchmark interaction energies for all 14 glycidol dimer structures. These energies are calculated at the DF-MP2/(AVQZ,AV5Z)+ $\Delta$ CCSD(T)/AVTZ level of theory including the counterpoise correction.

Table II: Calculated monomer deformation energies, binding energies  $(D_e)$ , vibrational zero-point energy differences  $(\Delta ZPE)$ , and dissociation energies  $(D_0)$  at the DF-MP2/(AVQZ,AV5Z)+ $\Delta CCSD(T)/AVTZ$  level (in kcal mol<sup>-1</sup>) of the glycidol dimer.

		_		ahina		
Structure	$E_{\mathrm{int}}$	$E_{\text{deformation}}$	$D_{\rm e}$	$\Delta D_{ m e}^{ m chira}$	$\Delta \mathrm{ZPE}$	$D_0$
HOM811	-14.355	4.238	10.117	0.571	1.049	9.068
HET811	-15.975	6.429	9.546		1.114	8.432
HOM812	-12.567	2.966	9.601	0.952	1.084	8.517
HET812	-11.098	2.449	8.649		0.881	7.768
HOM822	-11.802	2.310	9.492	0.315	1.253	8.239
HET822	-11.621	2.444	9.177		1.138	8.039
HOM511	-10.048	1.258	8.790	-1.050	1.137	7.653
HET511	-11.522	1.682	9.840		1.305	8.535
HOM512	-9.980	1.760	8.220	0.075	0.958	7.262
HET512	-9.887	1.742	8.145		0.940	7.205
HOM521	-10.259	2.237	8.022	-0.699	1.038	6.984
HET521	-10.996	2.275	8.721		1.201	7.520
HOM522	-12.249	2.622	9.627	0.680	1.334	8.293
HET522	-11.839	2.892	8.947		1.291	7.656

 $<sup>^{\</sup>rm a}$  Defined as  $\Delta D_{\rm e}^{\rm chir} = D_{\rm e,homodimer} - D_{\rm e,heterodimer}$ 

The chirodiastaltic energies  $\Delta E_{\rm chir}^{\rm int}$ , Eq. (2), in Table I show that the largest positive value belongs to the HOM811 and HET811 pair where the heterochiral conformer is preferred over the homochiral one as far as the interaction energy is concerned. The largest negative chirodiastaltic energy occurs for the HOM812 and HET812 pair that implies the homochiral structure is favored over its heterochiral counterpart.

All  $\Delta E_{\rm int}^{\rm CCSD(T)}$  corrections are in the 0.08-0.2 kcal/mol range, indicating that the DF-MP2/CBS method performs well for these hydrogen-bonded systems. Overall, the interaction energies at the minima range from -9.9 kcal/mol for HET512 to -16.0 kcal/mol for HET811, in an expected range for a system held together by two hydrogen bonds. The HOM811/HET811 pair clearly represents the most favorable configuration of two glycidol molecules, and most structures involving an 8-member hydrogen-bonded ring are slightly more stable than those with a 5-membered ring.

In contrast to our previous work<sup>8</sup> on the propylene oxide dimer, the monomer deformation contribution cannot be neglected for the glycidol complex because this molecule is much more flexible than propylene oxide. Not only the hydroxyl group can rotate around the C-O bond, but also the entire hydroxymethyl group can undergo a rotation around the C-C bond, giving more degrees of freedom to the glycidol molecule. Moreover, the intermolecular interaction, the driving force for possible deformation, is substantially stronger. The monomer deformation energy<sup>35</sup> is calculated as the difference between the energy of monomers in the dimer geometry and in the optimized monomer geometry<sup>35</sup> and it is always calculated at the same DF-MP2/(AVQZ,AV5Z)+ $\Delta$ CCSD(T)/AVTZ level as the interaction energy, but with monomer basis sets.

The resulting monomer deformation energies along with the binding energy values

$$D_e = \left| E^{\text{int}} + E^{\text{deformation}} \right| \tag{9}$$

for all 14 glycidol dimer structures are presented in Table II. As can be seen, the monomer deformation energies are in the 1-3 kcal/mol range for the glycidol dimer structures except for the HOM811 and HET811 complexes. Further investigation revealed that these relatively large deformation effects result from the fact that in an isolated glycidol molecule in the M1 configuration, the hydrogen atom of the hydroxyl group is attracted to the epoxide ring oxygen. Therefore, the OH···O contact, while not a perfect linear intramolecular hydrogen bond, is definitely a favorable interaction. When a glycidol molecule approaches another glycidol molecule, this favorable interaction is reduced to a different extent as the hydroxyl hydrogen atom rotates towards the oxygen atoms of the adjacent glycidol molecule. This conformational change is particularly pronounced for the HET811 structure, as evidenced by Fig. 3 which shows that the deformation energy strongly correlates with the sum of the two intramolecular nonbonded O(oxirane)-H(alcohol) distances, showing that the dominant energetic penalty incurred in the dimer is associated with the rotation of the hydroxyl hydrogen atoms away from the intramolecular OH···O contact. In addition, binding energies show that the HOM811 conformation has the most favorable interaction, which is in complete agreement with the previous studies that showed HOM811 as the global minimum<sup>2,7</sup>. Actually, the RR/SS diastereomer is the more stable one in all 8-membered ring structures. Overall, the inclusion of the monomer deformation energy has two interesting effects on the relative stability of different conformations in Table II. First, HOM811 becomes the global

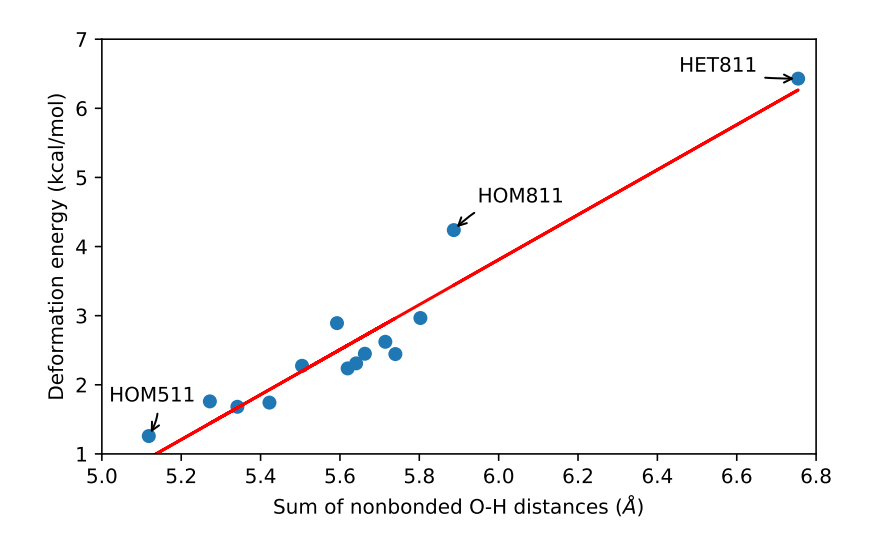


FIG. 3: Monomer deformation energies for all 14 glycidol dimer structures versus the sum of the two intramolecular nonbonded OH distances.

minimum as the HET811 structure, favored on the interaction energy grounds, requires a particularly large distortion of the monomers. Second, the binding energies for all 14 minima are in a narrower range than interaction energies, with no clear preference for the HOM811/HET811 pair (actually, HET511 is slightly more stable than HET811). It is interesting to note that the glycidol molecules adjust to their structures in the complex primarily by the hydrogen atom rotation around the C-O bond. The other possible torsional motion, the rotation of the whole hydroxymethyl group around the C-C bond, is less pronounced as all glycidol molecules in the complexes retain either their M1 or M2 conformation as illustrated in Fig. 1.

Table II also contains the dissociation energies  $D_0$ , obtained from  $D_e$  by the addition of the vibrational zero-point energy (ZPE) correction  $\Delta$ ZPE = ZPE(AB) – ZPE(A) – ZPE(B). The  $\Delta$ ZPE values for different structures are in a fairly narrow 0.9 – 1.3 kcal/mol range, and the ordering of  $D_0$  values for different structures follows the ordering of  $D_e$ .

#### B. Performance of approximate approaches

Method	MUE fo	r 14 int	eraction	MUE for 7 chirodiastaltic				
	ene	ergy val	ues	energies				
	AVDZ	$\operatorname{AVTZ}$	CBS	AVDZ	$\operatorname{AVTZ}$	CBS		
MP2	1.516	0.516	0.149	0.150	0.079	0.040		
CCSD(T)	1.810	0.665		0.146	0.057			
SAPT0	1.544	2.321		0.161	0.222			
SAPT2+3	0.939	0.390		0.073	0.082			

Table III: Mean unsigned errors of the interaction energy (kcal/mol) for the 14 structures of glycidol dimer for various methods and basis sets.

In the discussion that follows, we quantify the performance of some approximate electronic structure theories relative to our benchmark energies using two quantities: the mean unsigned error (MUE) for all 14 interaction energies at the minima and the MUE for the 7 chirodiastaltic energies. Table III presents the comparison the resulting errors for

Method	MUE for 14 interaction	MUE for 7 chiro-		
	energy values	diastaltic energies		
B3LYP-D3(BJ)	0.219	0.105		
B3LYP-D3M(BJ)	0.133	0.100		
B3LYP-D3	0.117	0.108		
B3LYP-D3M	0.373	0.115		
BLYP-D3(BJ)	0.806	0.171		
BLYP-D3M(BJ)	0.254	0.166		
BLYP-D3	0.245	0.108		
BLYP-D3M	0.095	0.156		
PBE-D3(BJ)	0.416	0.170		
PBE-D3M(BJ)	0.450	0.171		
PBE-D3	0.222	0.142		
PBE-D3M	0.660	0.180		
PBE0-D3(BJ)	0.286	0.106		
PBE0-D3M(BJ)	0.256	0.104		
PBE0-D3	0.112	0.098		
PBE0-D3M	0.295	0.111		

Table IV: Mean unsigned errors (MUE) of the interaction energy for 14 structures of the glycidol dimer in the AVTZ basis set using various DFT functionals. All energy values are in kcal  $\mathrm{mol}^{-1}$ . Error statistics are computed relative to the DF-MP2/(AVQZ,AV5Z)+ $\Delta$ CCSD(T)/AVTZ benchmark.

several wavefunction methods. As can be seen from this table, SAPT2+3 and MP2 have the smallest MUE values of interaction energies in the aug-cc-pVTZ basis set, but neither method is converged to CBS at this level. It can be concluded that the accuracy of the results is strongly dependent on both the method and the basis set, as large basis sets including diffuse functions are vital to get reliable results for hydrogen-bonded complexes<sup>36,37</sup>. Among the four methods shown in Table III, SAPT2+3 shows the most complete error cancellation between the RR(SS) and RS(SR) structures at the AVDZ level, which leads to an MUE of 0.073 kcal/mol for the chirodiastaltic energy. At the AVTZ level, the chirodiastaltic energy errors from MP2 and CCSD(T) become slightly smaller.

The MUE values for different dispersion-corrected DFT variants relative to the DF-MP2/(AVQZ,AV5Z)+ $\Delta$ CCSD(T)/AVTZ benchmark are listed in Table IV both for the interaction energy and the chirodiastaltic energy, as computed in the aug-cc-pVTZ basis set. As this table shows, the BLYP-D3M, PBE0-D3, and B3LYP-D3 functionals perform well for glycidol dimer complexes with the MUE of 0.095, 0.112, and 0.117 kcal/mol, respectively. However, in contrast to the MUE values for the interaction energy, the most complete error cancellation for chirodiastaltic energy occurs in the PBE0-D3 dispersion-corrected functional, followed by the B3LYP-D3M(BJ) and PBE0-D3M(BJ) ones.

#### C. SAPT and F-SAPT results

Table V shows the interaction energy components calculated using the SAPT0 and SAPT2+3<sup>14,22</sup> approaches and the resulting chirodiastaltic energies in the aug-cc-pVTZ basis set. Using SAPT provides the splitting of the total interaction energy into electrostatics, exchange, induction, and dispersion, which can be analyzed individually. All 14 dimer structures have considerable large and negative electrostatic energies which are comparable in magnitude to the positive first-order exchange component. The large magnitude of electrostatic energy is not surprising for a hydrogen-bonded complex. The exchange part compensates the electrostatic part and as a result, the total interaction energy is dominated by the two remaining terms, induction and dispersion.

The comparison of SAPT0 and SAPT2+3 reveals that the former method overestimates the binding (gives interaction energies that are too negative). However, the SAPT0 chirodiastaltic energies are in reasonably good agreement with SAPT2+3 (and with the benchmark values in Table I), which is important as our subsequent F-SAPT difference analysis is performed at the SAPT0 level of theory. The biggest differences between SAPT0 and SAPT2+3 arise from the first-order exchange, which is more repulsive by 2.7 - 4.1 kcal/mol at the higher theory level. The electrostatic energy is also generally less negative for SAPT2+3, but by a smaller amount, up to 1.2 kcal/mol. On the other hand, the SAPT2+3 energy decomposition gives stronger attraction in the induction and dispersion parts, with the respective differences in the 0.5 - 0.8 and 1.0 - 1.5 kcal/mol ranges.

Figures. 4–10 show the functional-group SAPT (F-SAPT) difference analysis using the decomposition defined in Eqs. (7) and (8). Here, F-SAPT was applied at the SAPT0 level to evaluate the components of interaction energies and chirodiastaltic energies for all 14 glycidol dimer structures. F-SAPT allowed us to compute the SAPT

Structure Els	. Exch.	Ind.	Disp.	SAPT0	$\Delta E_{ m chir}^{ m int}$	Structure	Elst.	Exch.	Ind.	Disp.	SAPT2+3	$\Delta E_{ m chir}^{ m int}$
HOM811 -20.6	52 19.683	-7.612	-8.523	-17.104	1.725	HOM811	-19.869	23.280	-8.367	-9.813	-14.769	1.690
HET811 -22.6	77 21.663	-8.703	-9.111	-18.829		HET811	-21.922	25.509	-9.546	-10.499	-16.459	
HOM812 -19.2	96 19.755	-7.082	-8.450	-15.073	-1.196	HOM812	-18.629	23.218	-7.791	-9.753	-12.955	-1.391
HET812 -16.5	37 16.152	-6.110	-7.382	-13.877		HET812	-15.378	18.819	-6.614	-8.391	-11.564	
HOM822 -18.6	55 20.836	-6.711	-9.471	-14.002	0.044	HOM822	-18.480	24.654	-7.452	-10.938	-12.216	-0.206
HET822 -18.0	90 19.411	-6.437	-8.930	-14.046		HET822	-17.616	22.964	-7.122	-10.235	-12.010	
HOM511 -17.5	43 20.400	-6.194	-8.688	-12.025	1.890	HOM511	-17.685	24.304	-6.946	-10.053	-10.380	1.575
HET511 -20.0	58 22.614	-6.890	-9.582	-13.915		HET511	-19.872	26.570	-7.643	-11.010	-11.955	
HOM512 -15.2	77 16.209	-5.012	-7.743	-11.824	-0.069	HOM512	-15.088	19.158	-5.550	-8.816	-10.296	-0.209
HET512 -16.2	41 16.933	-5.516	-6.931	-11.755		HET512	-15.893	19.937	-6.103	-8.028	-10.087	
HOM521 -18.1	62 19.766	-6.637	-7.136	-12.168	0.968	HOM521	-17.998	23.250	-7.359	-8.386	-10.492	0.877
HET521 -19.1	45 22.034	-6.934	-9.091	-13.136		HET521	-19.241	26.151	-7.754	-10.526	-11.369	
HOM522 -19.5	39 20.807	-6.378	-9.704	-14.814	-0.686	HOM522	-19.125	24.476	-7.064	-11.064	-12.778	-0.452
HET522 -18.7	67 20.866	-6.248	-9.978	-14.128		HET522	-18.624	24.696	-6.961	-11.437	-12.326	

Table V: Interaction energy components for all 14 optimized glycidol structures computed with SAPT0 (left) and SAPT2+3 (right) in the AVTZ basis set, along with the resulting chirodiastaltic energies. All values are in units of kcal/mol.

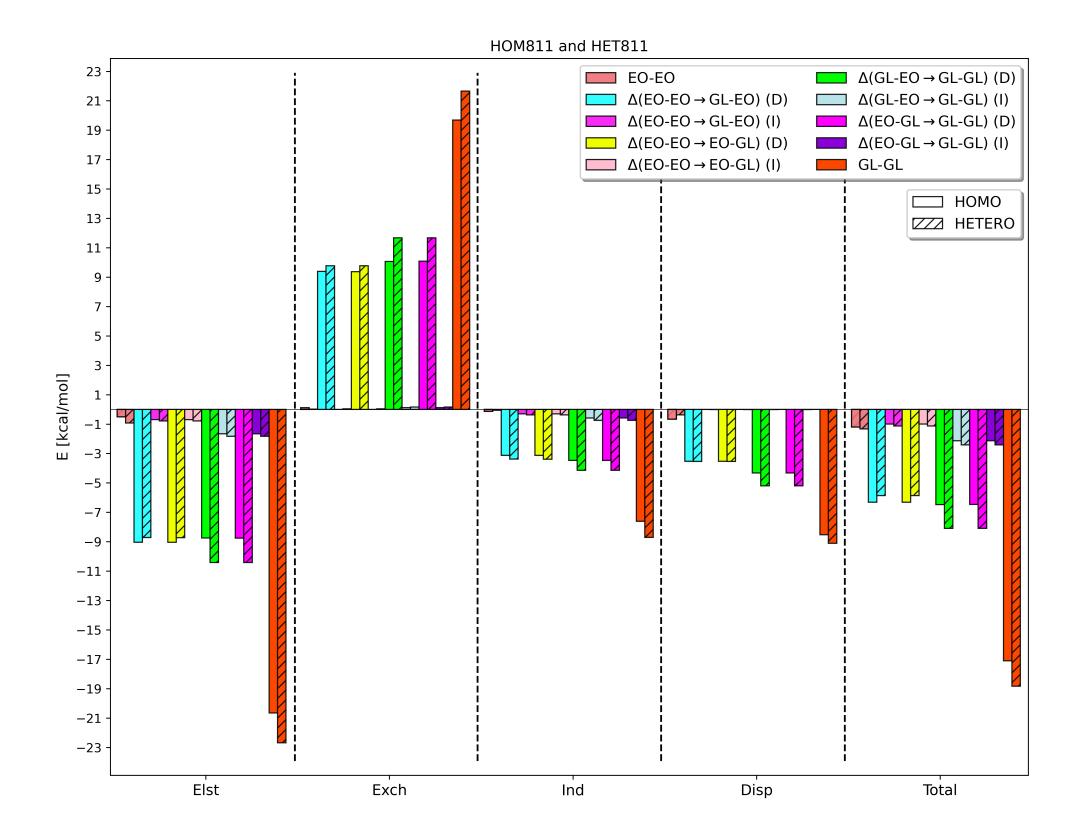


FIG. 4: Interaction energy components for the HOM811/HET811 pair of glycidol dimer structures as predicted by the F–SAPT difference analysis at the SAPT0/AVTZ level of theory. The bars marked EO-EO denote the energy components for the ethylene oxide (EO) dimer, which in subsequent steps is expanded into the glycidol dimer by replacing one hydrogen atom at a time by a -CH<sub>2</sub>OH functional group, as explained in detail in the text. The effects of this replacement are partitioned into the direct energy difference (denoted "D") between the Molecule-CH<sub>2</sub>OH and Molecule-H interactions and the indirect effect (denoted "I") stemming from an altered interaction with the ethylene-oxide backbone.

component contributions from each pair of user-defined functional groups, which in this case are the epoxide ring

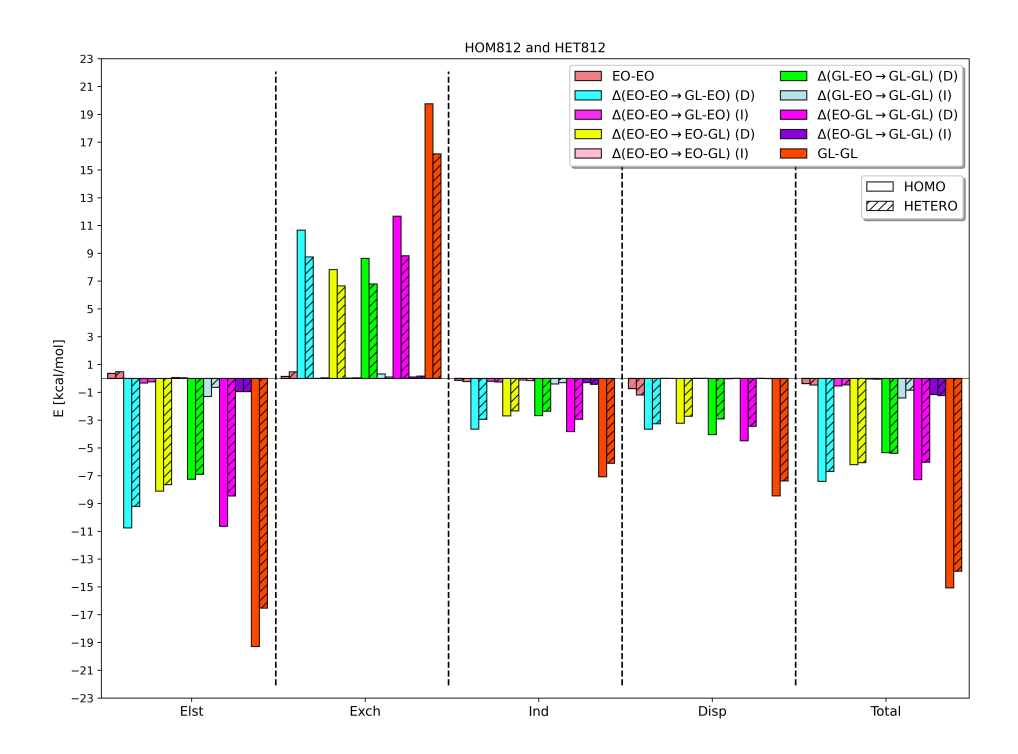


FIG. 5: Interaction energy components for the HOM812/HET812 pair of glycidol dimer structures as predicted by the F–SAPT difference analysis at the SAPT0/AVTZ level of theory. The bars marked EO-EO denote the energy components for the ethylene oxide (EO) dimer, which in subsequent steps is expanded into the glycidol dimer by replacing one hydrogen atom at a time by a -CH<sub>2</sub>OH functional group, as explained in detail in the text. The effects of this replacement are partitioned into the direct energy difference (denoted "D") between the Molecule-CH<sub>2</sub>OH and Molecule-H interactions and the indirect effect (denoted "I") stemming from an altered interaction with the ethylene-oxide backbone.

and the hydroxymethyl. The hydroxymethyl groups were sequentially added to a reduced structure featuring two achiral ethylene oxide molecules. Specifically, the -CH<sub>2</sub>OH group replaced a hydrogen atom pointed exactly in the same direction as the -CH<sub>2</sub>OH carbon atom, with the distance optimized at the DF-MP2/AVTZ level, keeping the remaining part of the complex invariant. There are two distinct orderings in which the hydroxymethyl groups are added to form the glycidol dimer out of the ethylene oxide dimer. Except for the symmetric dimer structures such as HET811, these two orderings are not equivalent and the F-SAPT differences for both orderings are presented in Figs. 4–10. Each F-SAPT difference is split into the direct and indirect effects of the -H  $\rightarrow$  -CH<sub>2</sub>OH substitution. The direct energetic effect refers to the difference between the interaction of the -CH<sub>2</sub>OH group with the entire other molecule and the corresponding interaction of its replacement -H atom. The remaining indirect effect is defined as the energy difference brought by the oxirane backbone, whose geometry does not change upon the -H  $\rightarrow$  -CH<sub>2</sub>OH replacement but the electron density does. Thus, it is the difference between the interaction of the entire other molecule and the oxirane backbone in glycidol versus the same oxirane backbone in ethylene oxide.

Figures 4–10 illustrate that the glycidol dimer structures are much more stable than their ethylene oxide dimer counterparts, as the increase in the attractive electrostatic, induction, and dispersion interactions is not nearly compensated by the growth in the repulsive exchange interaction upon the  $^{-}$ H  $\rightarrow$  -CH<sub>2</sub>OH replacement. In sharp contrast with the propylene oxide dimer<sup>8</sup>, the induction energy is very important for glycidol complexes, providing nearly the same amount of net attraction as the dispersion energy. The HOM811 and HET811 data in Figs. 4–10 reveal that the direct effects are similar each time the -CH<sub>2</sub>OH group is added, as in each addition one new hydrogen bond is formed. This is the common trend for all 8-membered rings, and it is completely different from the behavior of 5-membered ring structures. Among the 8-membered rings, in particular for the HOM811 and HET811 pair, the changes for the two possible pathways (Fig. 2) are highly consistent since these particular structures are close to symmetric. In the case of HOM822, there is no symmetry and the results for the two orderings are not exactly equal, but the trends of the direct and indirect energetic effects are similar to what we see for HOM811 and HET811. In other words, each

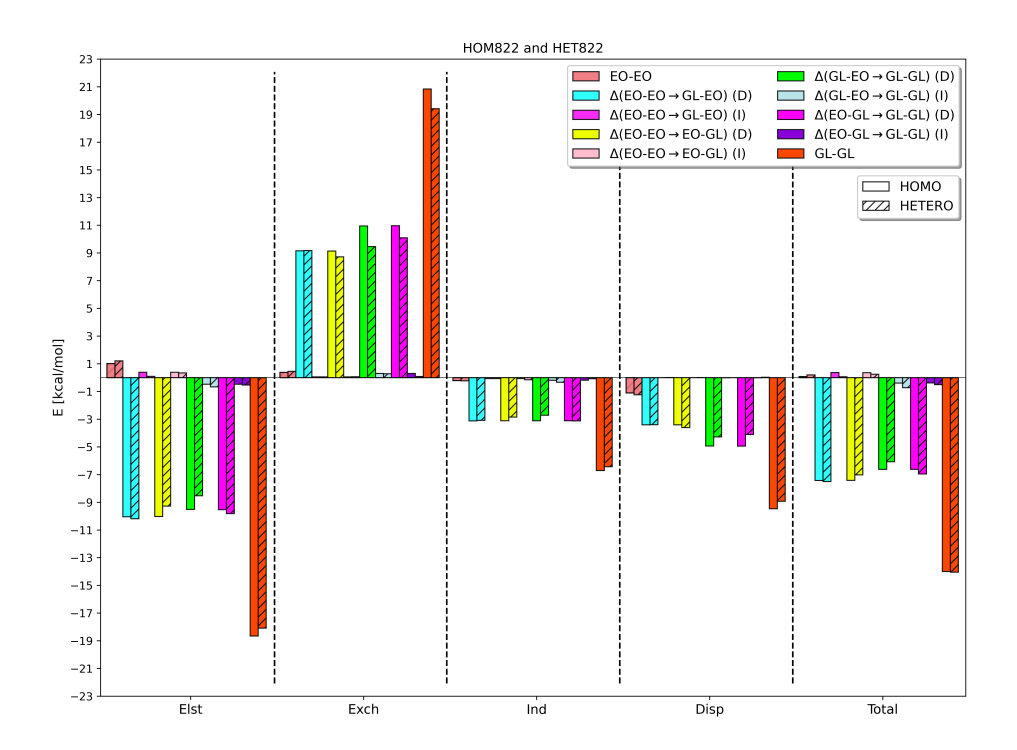


FIG. 6: Interaction energy components for the HOM822/HET822 pair of glycidol dimer structures as predicted by the F-SAPT difference analysis at the SAPT0/AVTZ level of theory. The bars marked EO-EO denote the energy components for the ethylene oxide (EO) dimer, which in subsequent steps is expanded into the glycidol dimer by replacing one hydrogen atom at a time by a -CH<sub>2</sub>OH functional group, as explained in detail in the text. The effects of this replacement are partitioned into the direct energy difference (denoted "D") between the Molecule-CH<sub>2</sub>OH and Molecule-H interactions and the indirect effect (denoted "I") stemming from an altered interaction with the ethylene-oxide backbone.

-H  $\rightarrow$  -CH<sub>2</sub>OH replacement creates a relatively strong hydrogen bond (a large direct effect) and the two resulting bonds are similar in strength. If we look at the 5-membered rings, there is quite a distinct behavior of the F-SAPT differences. We have the option to choose which monomer in the EO-EO structure undergoes the -H  $\rightarrow$  -CH<sub>2</sub>OH replacement first. One of the orderings of adding the functional groups gives a hydrogen bond the first time and a second hydrogen bond the second time, while the other ordering gives no hydrogen bonds the first time and both hydrogen bonds the second time. This is expected as in the case of 5-membered rings, one of the oxygen atoms acts as a hydrogen bond donor and acceptor simultaneously. Moreover, by looking at the individual components in each figure, it becomes clear that the direct effects have much larger contributions to the total interaction energy than the indirect effects, especially for the homochiral structures. The indirect effects are quite small at all stages of substitution, especially the dispersion ones (indicating a near pairwise additivity of dispersion<sup>38</sup> for this system, similar to our earlier study<sup>8</sup>). The only noticeable indirect F-SAPT contributions arise from the electrostatic energy. In any case, the bulk of the chirodiastaltic energy comes from the direct effects of the hydroxymethyl group insertion.

It is quite difficult to ascribe the chirodiastaltic energies to individual F-SAPT differences. Figures 4–10 show that the addition of the -CH<sub>2</sub>OH groups flips the energetic ordering of quite a few HOM/HET pairs, showing that there is no correlation between the overall GL-GL chiral interaction energy differences and the corresponding differences between the EO-EO backbone arrangements. Figures 4–10 also show that for all pairs of diastereomeric structures, the contributions of all individual SAPT components to the chirodiastaltic energy are large. However, the differences in the first-order repulsive exchange energy are largely canceled by the attractive electrostatic, induction, and dispersion contributions. Altogether, the energetic ordering of the RR and RS diastereomers follows the ordering of the electrostatic contributions except for the HOM822/HET822 and HOM512/HET512 pairs.

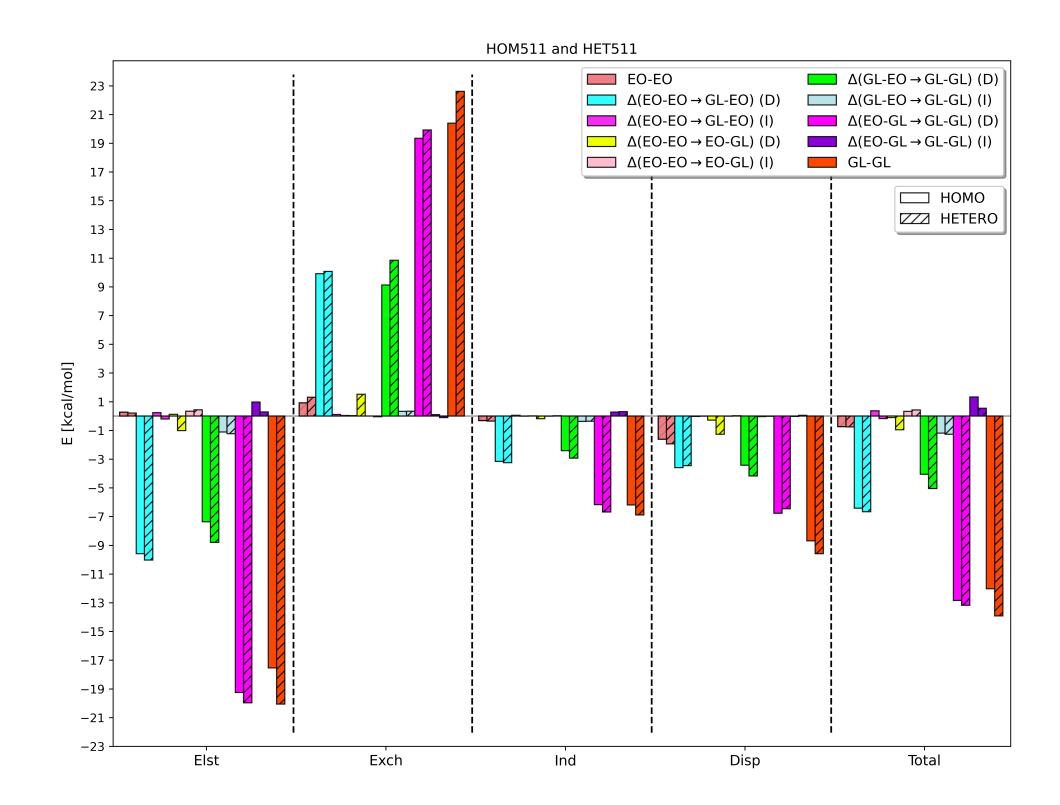


FIG. 7: Interaction energy components for the HOM511/HET511 pair of glycidol dimer structures as predicted by the F–SAPT difference analysis at the SAPT0/AVTZ level of theory. The bars marked EO-EO denote the energy components for the ethylene oxide (EO) dimer, which in subsequent steps is expanded into the glycidol dimer by replacing one hydrogen atom at a time by a -CH<sub>2</sub>OH functional group, as explained in detail in the text. The effects of this replacement are partitioned into the direct energy difference (denoted "D") between the Molecule-CH<sub>2</sub>OH and Molecule-H interactions and the indirect effect (denoted "I") stemming from an altered interaction with the ethylene-oxide backbone.

# D. Vibrational frequency shifts

We conclude this section by examining the frequency shifts of the normal modes of an isolated glycidol molecule resulting from the intermolecular interaction. We focus on the four most interesting modes in Fig. 11 that exhibit the largest shifts (the numerical data for all other modes are presented in the Supporting Information). They are the rotation of the -CH<sub>2</sub>OH group around the C-C bond, the rotation of the alcohol hydrogen atom around the C-O bond, the C-C-O bending involving the hydroxyl group oxygen, and the O-H stretching, corresponding to  $\nu_1 = 155.0$  cm<sup>-1</sup>,  $\nu_4 = 458.9$  cm<sup>-1</sup>,  $\nu_5 = 623.6$  cm<sup>-1</sup>, and  $\nu_{27} = 3778.4$  cm<sup>-1</sup>, respectively.

For the O-H stretching mode, the frequencies in the dimers are always lower relative to the monomer (red-shifted) which is the typical characteristic of the hydrogen bonds. An examination of the frequency values for the stretching mode reveals a clear difference between the structures with 8-membered rings and those with 5-membered rings. In the 8-membered ring structures, both hydrogen bonds are similar because they are formed with the same type of oxygen atom acceptor belonging to the epoxide ring. Therefore, the differences between the two frequency shifts are small. However, for the 5-membered rings these differences are larger because the two hydrogen bonds are not equivalent: one of the acceptor oxygens belongs to the epoxide ring while the second acceptor is the alcohol group oxygen.

We now turn to the  $\nu_5$  normal mode that describes the C-C-O bending motion involving a ring carbon, a non-ring carbon, and the hydroxyl oxygen. There is an interesting pattern in this mode for both 8-membered and 5-membered rings: when the two molecules in a dimer are in the M1 conformation from Fig. 1, both frequency shifts are small. Once one of the monomers in the complex has the M1 conformation and the other the M2 one, there will be one big shift and one small shift in frequencies. Finally, when both monomers in the dimer are in the M2 conformation, we

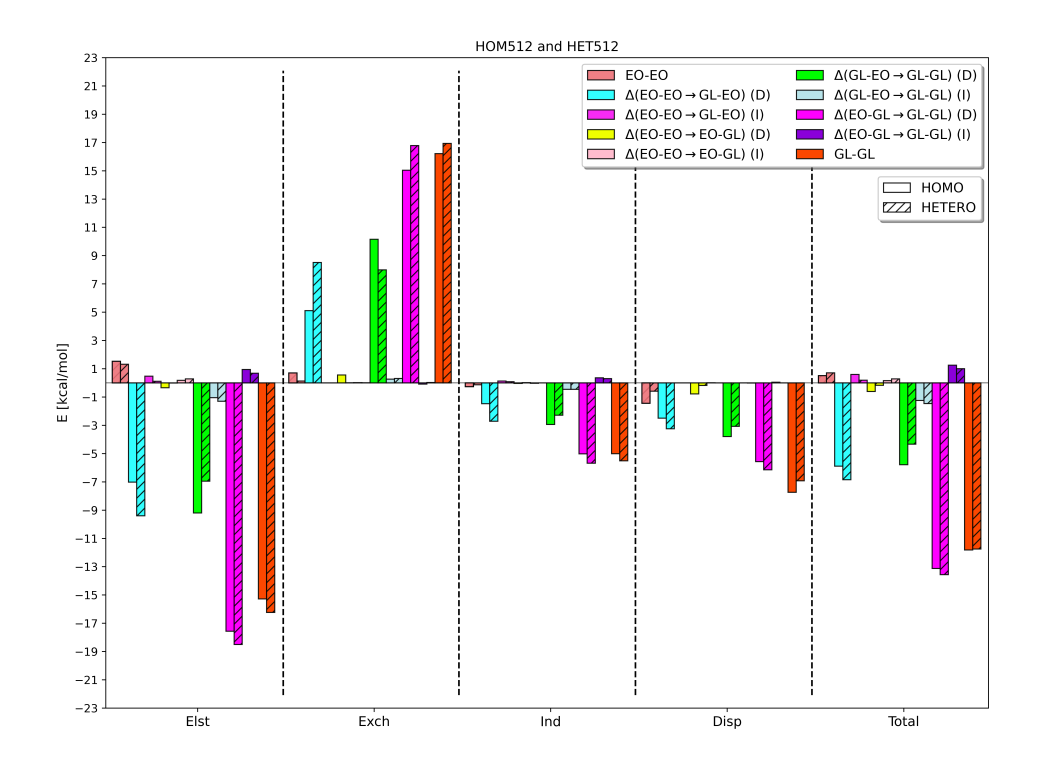


FIG. 8: Interaction energy components for the HOM512/HET512 pair of glycidol dimer structures as predicted by the F–SAPT difference analysis at the SAPT0/AVTZ level of theory. The bars marked EO-EO denote the energy components for the ethylene oxide (EO) dimer, which in subsequent steps is expanded into the glycidol dimer by replacing one hydrogen atom at a time by a -CH<sub>2</sub>OH functional group, as explained in detail in the text. The effects of this replacement are partitioned into the direct energy difference (denoted "D") between the Molecule-CH<sub>2</sub>OH and Molecule-H interactions and the indirect effect (denoted "I") stemming from an altered interaction with the ethylene-oxide backbone.

see two large frequency shifts. Among the two possible minimum structures for an isolated glycidol molecule, M1 is the global minimum while M2 is the next accessible local minimum; note that we are comparing all frequency shifts against the global minimum monomer conformation M1. Because of this observation, we calculated the normal modes for the local minimum M2 structure and found that the  $\nu_5$  mode has a frequency of 521.7 cm<sup>-1</sup>, a -102.0 cm<sup>-1</sup> shift relative to the global minimum, and a similar shift to those observed in Fig. 11. Thus, the large  $\nu_5$  shifts displayed in Fig. 11 arise entirely out of the monomer transformation from the M1 conformation to the M2 one, and any effects of the intermolecular interaction, beyond facilitating this transformation, are minor.

The next important frequency in Fig. 11 is  $\nu_4$  which corresponds to the H atom of the hydroxyl group rotating around the C-O bond. As can be seen, the frequency shifts are large and positive (blue-shifted) for this mode. At the equilibrium, there is a hydrogen bond between the H atom of the alcohol group and the O atom of the adjacent glycidol monomer, however, when this H atom starts to rotate out of position, it breaks the hydrogen bond; as a result, the energy increases and this leads to a steeper potential well and an increase in the frequency. As a result, we observe a larger vibrational frequency in the dimer than in the monomer, and the frequency shifts themselves are large too, big enough to reorder the frequencies of normal modes relative to the isolated monomer. It is notable that one of the two  $\nu_4$  frequency shifts is particularly large, up to about 400 cm<sup>-1</sup>, for all structures with 5-membered rings, indicating that a smaller ring is particularly sensitive to the distortion associated with the H atom rotation.

The last normal mode highlighted in Fig. 11 is  $\nu_1$ , which is a low-energy torsional mode corresponding to the rotation around the C-C bond between the oxirane backbone and the hydroxymethyl group. In the case of the M1 monomer structure, the lowest harmonic vibrational mode has been estimated around 155.0 cm<sup>-1</sup>, which is in an acceptable agreement with the experimental value of 145(15) cm<sup>-1</sup>.<sup>26</sup> Moreover, this C-C torsional mode frequency is in good agreement with side bands of the experimental gas-phase spectrum in Fig. 1 of Ref. 2.

As Fig. 11 shows, almost all of the  $\nu_1$  frequencies are blue-shifted. The examination of this normal mode in the

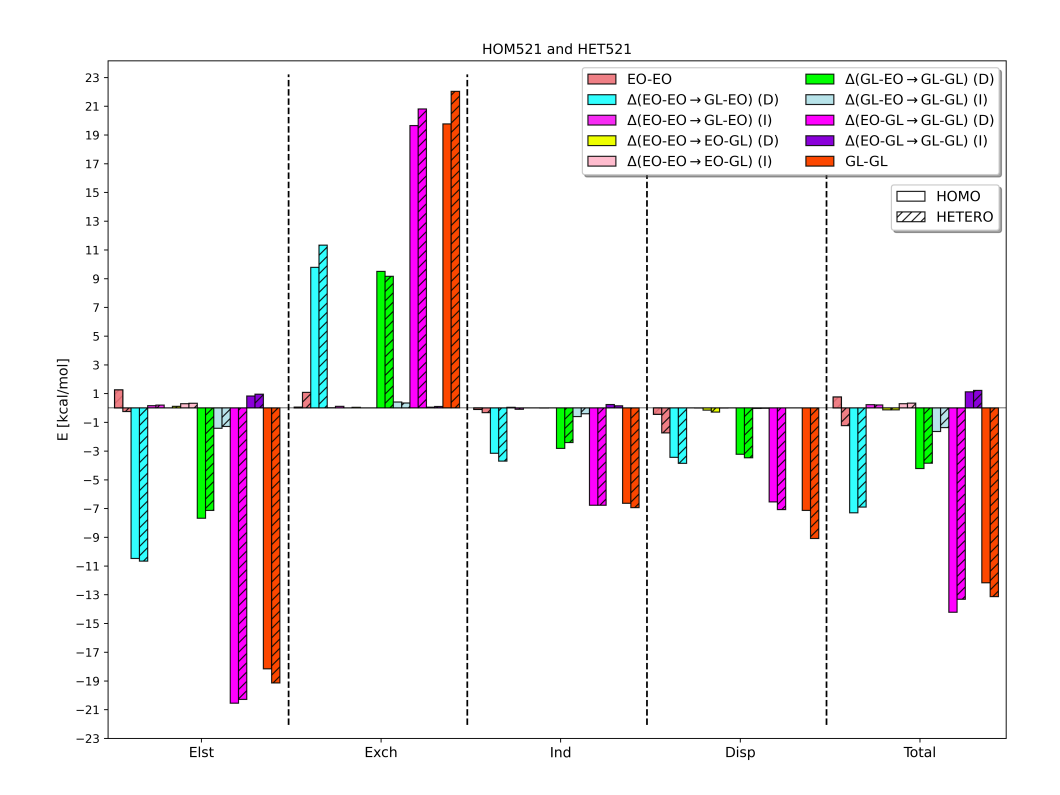


FIG. 9: Interaction energy components for the HOM521/HET521 pair of glycidol dimer structures as predicted by the F-SAPT difference analysis at the SAPT0/AVTZ level of theory. The bars marked EO-EO denote the energy components for the ethylene oxide (EO) dimer, which in subsequent steps is expanded into the glycidol dimer by replacing one hydrogen atom at a time by a -CH<sub>2</sub>OH functional group, as explained in detail in the text. The effects of this replacement are partitioned into the direct energy difference (denoted "D") between the Molecule-CH<sub>2</sub>OH and Molecule-H interactions and the indirect effect (denoted "I") stemming from an altered interaction with the ethylene-oxide backbone.

complex structures shows that this is a mixed torsional mode. As a result, instead of finding two frequencies with a pronounced C-C torsional character, there were three such modes. This means that the  $\nu_1$  mode is mixed with something else in the dimer (specifically, with an intermolecular vibration), and that is why there are three frequency shift bars for  $\nu_1$  in Fig. 11. Two of these bars always indicate blue shifts, showing that the intramolecular torsional motion is somewhat hindered by the intermolecular hydrogen bonding, while the last frequency is either unchanged or slightly red-shifted.

#### IV. SUMMARY

In this study, we have elucidated the chiral discrimination effects in the interaction between two glycidol molecules using high-accuracy ab initio calculations. These weak noncovalent interactions give rise to 14 diastereomeric structures, consisting of seven homochiral and seven heterochiral conformations, categorized into 8-membered ring and 5-membered ring structures, occurring in pairs that exhibit the same pattern of hydrogen bonding and the same monomer conformations. The effects of chirality of the glycidol molecules lead to diastereomeric energy differences between homo- and heterochiral complexes in the range of 0.1 - 1.6 kcal/mol for the interaction energy and 0.1 - 1.1 kcal/mol for the binding energy (the latter includes monomer deformation). The geometries of dimers were taken from Ref. 7 and reoptimized at the DF-MP2 level with the AVTZ basis set, and the benchmark interaction energy values for all 14 structures were calculated at the DF-MP2 level and extrapolated to the complete basis set limit from AVQZ and AV5Z in the standard  $X^{-3}$  extrapolation of the correlation part<sup>39</sup>, with an added  $\Delta$ CCSD(T) correction computed in the AVTZ basis set.

Both supermolecular approaches such as dispersion-corrected density functional theory (DFT-D) $^{30,40}$  and pertur-

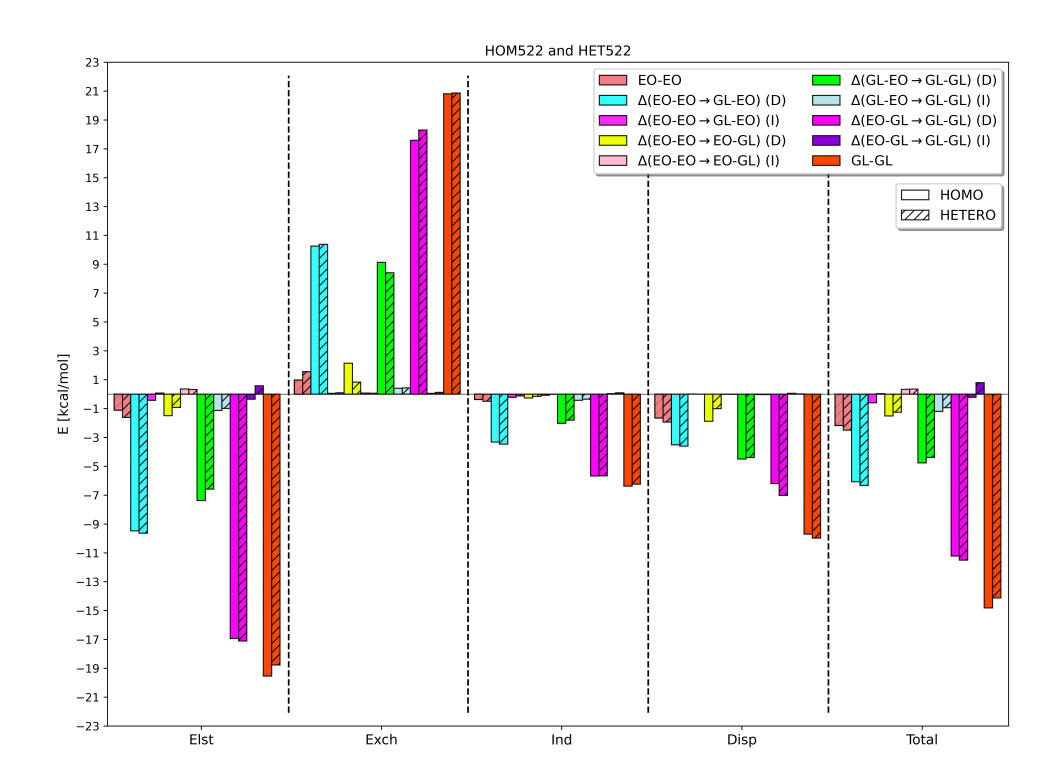


FIG. 10: Interaction energy components for the HOM522/HET522 pair of glycidol dimer structures as predicted by the F-SAPT difference analysis at the SAPT0/AVTZ level of theory. The bars marked EO-EO denote the energy components for the ethylene oxide (EO) dimer, which in subsequent steps is expanded into the glycidol dimer by replacing one hydrogen atom at a time by a -CH<sub>2</sub>OH functional group, as explained in detail in the text. The effects of this replacement are partitioned into the direct energy difference (denoted "D") between the Molecule-CH<sub>2</sub>OH and Molecule-H interactions and the indirect effect (denoted "I") stemming from an altered interaction with the ethylene-oxide backbone.

bative methods such as SAPT<sup>14</sup> were used to calculate the interaction energies in the 14 glycidol dimer structures. Among different flavors of DFT+D, the BLYP-D3M, B3LYP-D3, and PBE0-D3 variants perform very well on the interaction energies with the lowest average error around 0.1 kcal/mol. As the MUE values show, the chirodiastaltic energies benefit from error cancellation between the homo- and heterochiral dimer structures for most variants and methods considered. Approximate approaches such as DFT+D recover the chiral energy differences with an accuracy of about 0.1 kcal/mol.

Symmetry-adapted perturbation theory leads to a systematic overbinding of all glycidol dimer structures, but at the more accurate SAPT2+3 level, the overbinding is less severe than at the SAPT0 level. Both SAPT0 and SAPT2+3 show similar interaction energy trends and nearly always predict the correct sign for the chirodiastaltic energy values. The acceptably accurate SAPT0 description of the chirodiastaltic energy can be used to get insight into the origins of the chiral recognition in the glycidol complexes. Accordingly, we fine-grained the SAPT data by performing F-SAPT calculations with each glycidol molecule partitioned into the oxirane backbone and the hydroxymethyl group. Moreover, we carried out a difference analysis in which the effects of a hydrogen atom replacement in ethylene oxide by a hydroxymethyl group in glycidol can be singled out and analyzed. In this way, the direct (functional group interaction) and indirect (backbone electronic reorganization) effects of the -H  $\rightarrow$  -CH<sub>2</sub>OH substitution are distinguishable. The SAPT results show a typical pattern for a complex held together by two hydrogen bonds: while the electrostatic energy is the largest attractive term, it is more than offset by the repulsive first-order exchange energy so that the total first-order effect is repulsive. In second order, in addition to a sizable dispersion energy, nearly the same amount of stabilization is provided by induction. Moreover, the direct effects of the -H→-CH<sub>2</sub>OH substitution in the F-SAPT energy differences overwhelm the indirect effects. The dominant contributions in the F-SAPT difference analysis arise from the hydrogen bond formation upon substitution. For the 8-membered ring structures, the hydrogen bonds are always formed one at a time, while for the 5-membered ring ones the two bonds

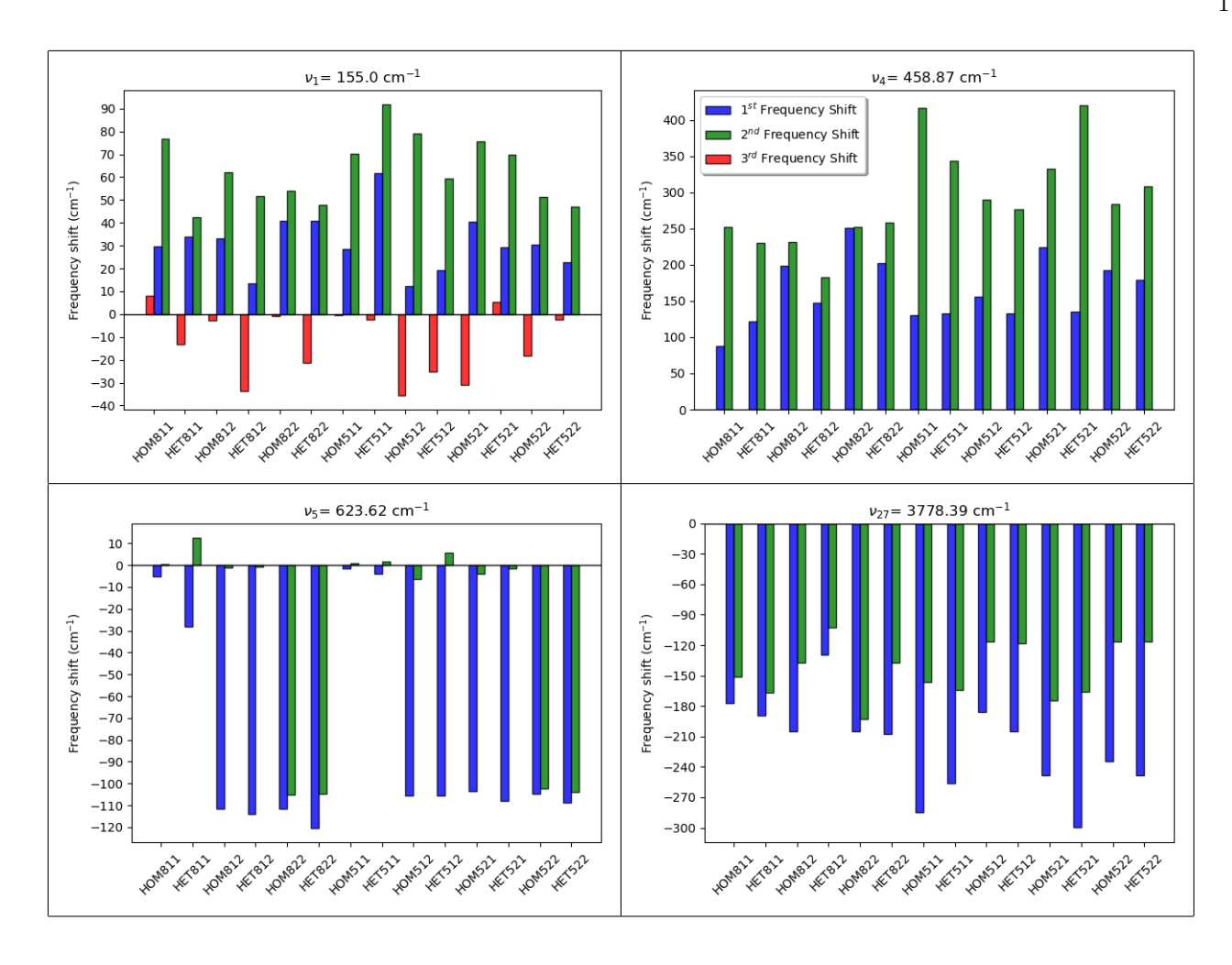


FIG. 11: Vibrational frequency shifts of the most important normal modes of the 14 glycidol dimer structures relative to the isolated monomer frequencies. Because of the existence of two identical monomers, there are two frequency shifts pertinent to each monomer in the complex. The  $\nu_1$  mode is strongly coupled to an intermolecular mode and heavily contributes to the three frequencies shown.

can be formed one at a time or both at once, depending on which -CH<sub>2</sub>OH group is added first.

As a result of the intermolecular interaction, two distinguishable shifts of each vibrational frequency of an isolated glycidol molecule are obtained from calculations. These two frequency shifts were analyzed at the DF-MP2/AVTZ level for all 14 structures. The modes with the largest shifts caused by the noncovalent interactions are arising from the C-C torsional mode (where one of the C atoms is out of the epoxide ring), the C-O torsional mode within the -CH<sub>2</sub>OH group, the C-C-O bending mode (both C and O atoms are out of the epoxide ring), and the O-H stretching mode. The O-H stretching frequencies are around  $3600 - 3700 \text{ cm}^{-1}$ , in acceptable agreement with experiment<sup>26</sup>. Because of the nature of the hydrogen bonding in the 8-membered and 5-membered ring structures, the differences between the two frequency shifts in this O-H stretching mode are small for the 8-membered ring conformations while there is a larger difference up to  $140 \text{ cm}^{-1}$  for the 5-membered ring structures. There was an interesting pattern in the C-C-O bending mode which makes it possible to distinguish which monomer conformations (M1, M2, or both) are present in the complex. Compared to the previously studied propylene oxide dimer<sup>8</sup>, the interaction energies, monomer flexibility effects, and frequency shifts are all much bigger due to the presence of two conventional O-H···O hydrogen bonds rather than the weaker C-H···O contacts.

#### SUPPORTING INFORMATION

Cartesian coordinates for the 14 optimized configurations of the glycidol dimer. Vibrational frequencies for all 14 complexes and for an isolated glycidol molecule.

## ACKNOWLEDGMENTS

This work was supported by the U.S. National Science Foundation awards CHE-1351978 and CHE-1955328. A part of the calculations was carried out at the Auburn University Hopper Research Cluster. We thank Dr. Assimo Maris for supplying us with the Cartesian geometries from Ref. 7.

#### REFERENCES

\* patkowsk@auburn.edu

- <sup>1</sup> Bailey, J.; Chrysostomou, A.; Hough, J. H.; Gledhill, T. M.; McCall, A.; Clark, S.; Ménard, F.; Tamura, M. Circular Polarization in Star-Formation Regions: Implications for Biomolecular Homochirality. *Science* **1998**, 281, 672–674.
- <sup>2</sup> Borho, N.; Suhm, M. A. Glycidol dimer: anatomy of a molecular handshake. Phys. Chem. Chem. Phys. 2002, 4, 2721–2732.
- <sup>3</sup> Borho, N.; Haber, T.; Suhm, M. A. Chiral self-recognition in the gas phase: the case of glycidol dimers. *Phys. Chem. Chem. Phys.* **2001**, *3*, 1945–1948.
- <sup>4</sup> Su, Z.; Borho, N.; Xu, Y. Chiral Self-Recognition: Direct Spectroscopic Detection of the Homochiral and Heterochiral Dimers of Propylene Oxide in the Gas Phase. J. Am. Chem. Soc. **2006**, 128, 17126–17131.
- <sup>5</sup> Yang, G.; Xu, Y. The effects of self-aggregation on the vibrational circular dichroism and optical rotation measurements of glycidol. *Phys. Chem. Chem. Phys.* **2008**, *10*, 6787–6795.
- <sup>6</sup> Thomas, J.; Sunahori, F. X.; Borho, N.; Xu, Y. Chirality Recognition in the Glycidol··· Propylene Oxide Complex: A Rotational Spectroscopic Study. *Chem. Eur. J.* **2011**, *17*, 4582−4587.
- Maris, A.; Giuliano, B. M.; Bonazzi, D.; Caminati, W. Molecular Recognition of Chiral Conformers: A Rotational Study of the Dimers of Glycidol. J. Am. Chem. Soc. 2008, 130, 13860–13861.
- <sup>8</sup> Hemmati, R.; Patkowski, K. Chiral Self Recognition: Interactions in Propylene Oxide Complexes. J. Phys. Chem. A 2019, 123, 8607–8618.
- <sup>9</sup> Chojecki, M.; Rutkowska-Zbik, D.; Korona, T. On the applicability of functional-group symmetry-adapted perturbation theory and other partitioning models for chiral recognition the case of popular drug molecules interacting with chiral phases. *Phys. Chem. Chem. Phys.* **2019**, *21*, 22491–22510.
- <sup>10</sup> King, A. K.; Howard, B. J. A microwave study of the hetero-chiral dimer of butan-2-ol. Chem. Phys. Lett. 2001, 348, 343–349.
- Portmann, S.; Inauen, A.; Lüthi, H. P.; Leutwyler, S. Chiral discrimination in hydrogen-bonded complexes. J. Chem. Phys. 2000, 113, 9577–9585.
- Burns, L. A.; Marshall, M. S.; Sherrill, C. D. Appointing silver and bronze standards for noncovalent interactions: A comparison of spin-component-scaled (SCS), explicitly correlated (F12), and specialized wavefunction approaches. J. Chem. Phys. 2014, 141, 234111.
- <sup>13</sup> Kodrycka, M.; Patkowski, K. Platinum, gold, and silver standards of intermolecular interaction energy calculations. J. Chem. Phys. 2019, 151, 070901.
- Jeziorski, B.; Moszyński, R.; Szalewicz, K. Perturbation Theory Approach to Intermolecular Potential Energy Surfaces of van der Waals Complexes. Chem. Rev. 1994, 94, 1887–1930.
- Hohenstein, E. G.; Sherrill, C. D. Wavefunction Methods for Noncovalent Interactions. WIREs Comput. Mol. Sci. 2012, 2, 304–326.
- <sup>16</sup> Patkowski, K. Recent developments in symmetry-adapted perturbation theory. WIREs Comput. Mol. Sci. 2020, 10, e1452.
- Parrish, R. M.; Parker, T. M.; Sherrill, C. D. Chemical Assignment of Symmetry-Adapted Perturbation Theory Interaction Energy Components: The Functional-Group SAPT Partition. J. Chem. Theory Comput. 2014, 10, 4417–4431.
- Parrish, R. M.; Sherrill, C. D. Quantum-Mechanical Evaluation of π-π versus Substituent-π Interactions in π Stacking: Direct Evidence for the Wheeler-Houk Picture. J. Am. Chem. Soc. 2014, 136, 17386–17389.
- <sup>19</sup> Bakr, B. W.; Sherrill, C. D. Analysis of transition state stabilization by non-covalent interactions in the Houk? List model of organocatalyzed intermolecular Aldol additions using functional-group symmetry-adapted perturbation theory. *Phys. Chem. Phys.* 2016, 18, 10297–10308.
- Bakr, B. W.; Sherrill, C. D. Analysis of transition state stabilization by non-covalent interactions in organocatalysis: application of atomic and functional-group partitioned symmetry-adapted perturbation theory to the addition of organoboron reagents to fluoroketones. *Phys. Chem. Chem. Phys.* **2018**, *20*, 18241–18251.

- <sup>21</sup> Smith, D. G. A.; Burns, L. A.; Patkowski, K.; Sherrill, C. D. Revised Damping Parameters for the D3 Dispersion Correction to Density Functional Theory. J. Phys. Chem. Lett. 2016, 7, 2197–2203.
- <sup>22</sup> Parker, T. M.; Burns, L. A.; Parrish, R. M.; Ryno, A. G.; Sherrill, C. D. Levels of Symmetry Adapted Perturbation Theory (SAPT). I. Efficiency and Performance for Interaction Energies. J. Chem. Phys. 2014, 140, 094106.
- <sup>23</sup> Chojecki, M.; Rutkowska-Zbik, D.; Korona, T. Dimerization Behavior of Methyl Chlorophyllide a as the Model of Chlorophyll a in the Presence of Water Molecules—Theoretical Study. J. Chem. Inf. Model. 2019, 59, 2123–2140.
- <sup>24</sup> Ōki, M.; Murayama, T. Intramolecular Interaction between the Hydroxyl Group and the Oxirane Ring. Bull. Chem. Soc. Jpn. 1973, 46, 259–263.
- Oki, M.; Iwamura, H.; Murayama, T.; Oka, I. Intramolecular Interaction between the Hydroxyl Group and the Cyclopropane Ring. Bull. Chem. Soc. Jpn. 1969, 42, 1986–1991.
- Marstokk, K.-M.; Møllendal, H.; Stenstrøm, Y. Microwave Spectrum of Oxiranemethanol (Glycidol), the Assignment of a Second Hydrogen-Bonded Conformer and Conformational Composition in the Gas Phase and in Solution. Acta Chem. Scand. 1992, 46, 432–441.
- <sup>27</sup> Dunning Jr., T. H. Gaussian-Basis Sets for Use in Correlated Molecular Calculations. 1. The Atoms Boron through Neon and Hydrogen. J. Chem. Phys. 1989, 90, 1007–1023.
- <sup>28</sup> Kendall, R. A.; Dunning Jr., T. H.; Harrison, R. J. Electron Affinities of the 1st-Row Atoms Revisited Systematic Basis Sets and Wave Functions. J. Chem. Phys. **1992**, 96, 6796–6806.
- Rezac, J.; Hobza, P. Benchmark calculations of interaction energies in noncovalent complexes and their applications. Chem. Rev. 2016, 116, 5038–5071.
- <sup>30</sup> Grimme, S.; Antony, J.; Ehrlich, S.; Krieg, H. A Consistent and Accurate Ab Initio Parametrization of Density Functional Dispersion Correction (DFT-D) for the 94 Elements H-Pu. J. Chem. Phys. 2010, 132, 154104.
- <sup>31</sup> Grimme, S.; Ehrlich, S.; Goerigk, L. Effect of the Damping Function in Dispersion Corrected Density Functional Theory. J. Comput. Chem. 2011, 32, 1456–1465.
- <sup>32</sup> Werner, H.-J.; Knowles, P. J.; Knizia, G.; Manby, F. R.; Schütz, M. Molpro: a general-purpose quantum chemistry program package. WIREs Comput Mol Sci 2012, 2, 242–253.
- <sup>33</sup> Parrish, R. M.; Burns, L. A.; Smith, D. G. A.; Simmonett, A. C.; DePrince, III, A. E.; Hohenstein, E. G.; Bozkaya, U.; Sokolov, A. Yu.; Di Remigio, R.; Richard, R. M. et al. PSI4 1.1: An Open-Source Electronic Structure Program Emphasizing Automation, Advanced Libraries, and Interoperability. J. Chem. Theory Comput. 2017, 13, 3185–3197.
- <sup>34</sup> Parrish, R. M.; Sherrill, C. D. Spatial assignment of symmetry adapted perturbation theory interaction energy components: The atomic SAPT partition. J. Chem. Phys. 2014, 141, 044115.
- <sup>35</sup> Patkowski, K. Benchmark Databases of Intermolecular Interaction Energies: Design, Construction, and Significance. In *Annual Reports in Computational Chemistry*; Dixon, D. A., Ed.; Elsevier, Amsterdam, 2017; Vol. 13; pp 3–91.
- <sup>36</sup> Boese, A. D. Assessment of Coupled Cluster Theory and more Approximate Methods for Hydrogen Bonded Systems. J. Chem. Theory Comput. 2013, 9, 4403–4413.
- <sup>37</sup> Řezáč, J. Non-Covalent Interactions Atlas Benchmark Data Sets: Hydrogen Bonding. J. Chem. Theory Comput. 2020, 16, 2355–2368.
- <sup>38</sup> Grimme, S.; Hansen, A.; Brandenburg, J. G.; Bannwarth, C. Dispersion-Corrected Mean-Field Electronic Structure Methods. Chem. Rev. 2016, 116, 5105-5154.
- <sup>39</sup> Halkier, A.; Helgaker, T.; Jørgensen, P.; Klopper, W.; Koch, H.; Olsen, J.; Wilson, A. K. Basis-Set Convergence in Correlated Calculations on Ne, N<sub>2</sub>, and H<sub>2</sub>O. *Chem. Phys. Lett.* **1998**, *286*, 243–252.
- <sup>40</sup> Grimme, S. Semiempirical GGA-Type Density Functional Constructed with a Long-Range Dispersion Correction. J. Comput. Chem. 2006, 27, 1787–1799.

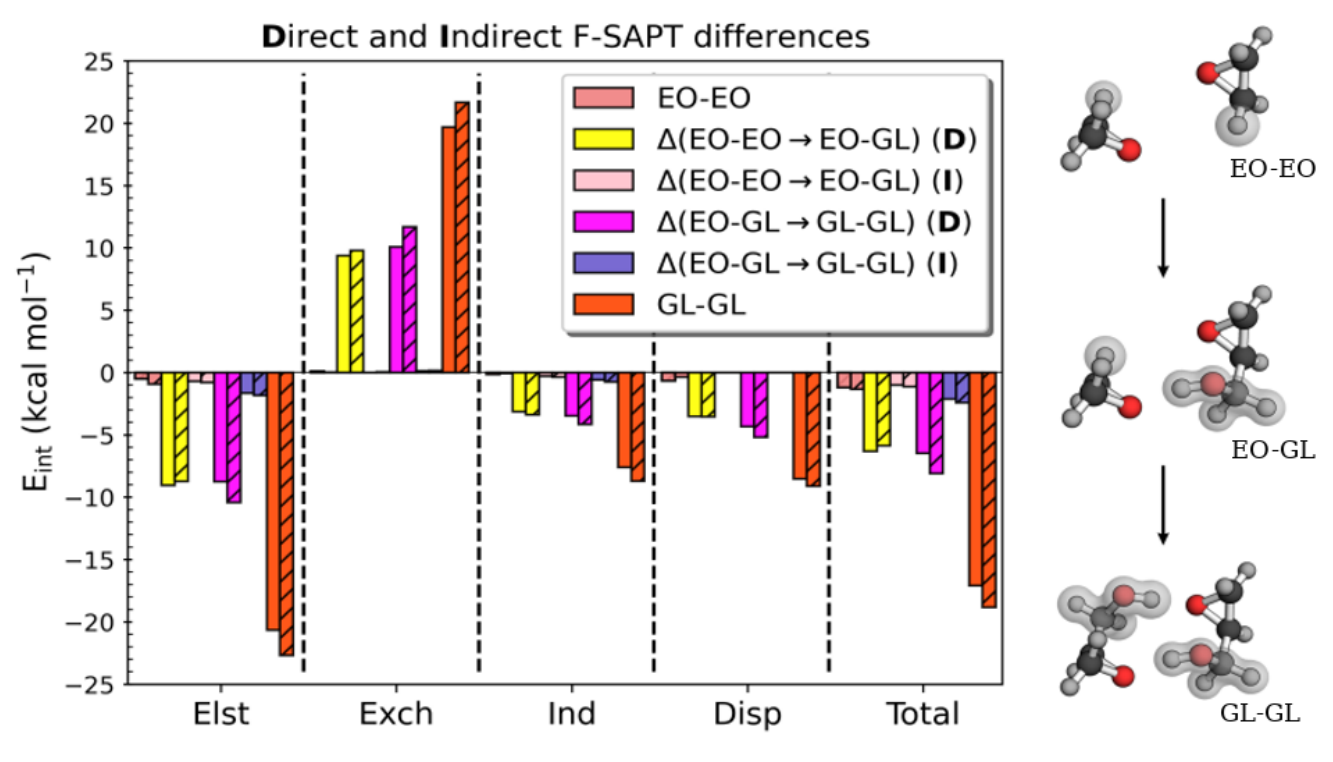


FIG. 12: TOC Graphic